Ba Deposition and Oxidation on θ-Al_2O_3/NiAl(100) Ultrathin Films. Part II: O_2(g) Assisted Ba Oxidation

Emrah Ozensoy, Charles H. F. Peden, and János Szanyi*

Institute for Interfacial Catalysis, Pacific Northwest National Laboratory, P.O. Box 999, MSIN K8−93, Richland, Washington 99352

Received: January 31, 2006; In Final Form: May 19, 2006

Ba deposition on a θ-Al_2O_3/NiAl(100) substrate and its oxidation with gas-phase O_2 at various surface temperatures are investigated using X-ray photoelectron spectroscopy (XPS), Auger electron spectroscopy (AES), and temperature programmed desorption (TPD) techniques. Oxidation of metallic Ba by gas-phase O_2 at 800 K results in the growth of 2D and 3D BaO surface domains. Saturation of a metallic Ba layer deposited on θ-Al_2O_3/NiAl(100) with O_2(g) at 300 K reveals the formation of BaO_2-like surface states. These metastable peroxide (O_2^{2-}) states are converted to regular oxide (O^{2-}) states at higher temperatures (800 K). In terms of thermal stability, BaO surface layers ($\theta_{Ba} < 5$ ML) that are formed by O_2(g) assisted oxidation on the θ-Al_2O_3/NiAl(100) substrate are significantly more stable (with a desorption/decomposition temperature of c.a. 1050 K) than the thick ($2 < \theta_{Ba} < 10$ ML) metallic/partially oxidized Ba layers prepared in the absence of gas-phase O_2, whose multilayer desorption features appear as low as 700 K.

1. Introduction

Ba metal and its oxides (BaO or BaO_2) have a wide variety of applications in the semiconductor and heterogeneous catalysis industries.[1−7] In particular, BaO has been utilized as the active NO_x storage component in NO_x storage reduction (NSR) catalysts[6,7] that are used to remove harmful NO_x emissions originating from lean-burn diesel engine operation. In this technology, the environmentally hazardous NO_x gases, emitted by the diesel engines operated in alternating lean (abundant in air and O_2) and rich (abundant in fuel, hydrocarbons, CO and H_2) conditions, are trapped and successively reduced to less hazardous N-containing compounds (such as N_2 and N_2O) by BaO and transition metal based NSR catalyst. In these NSR systems, NO(g), which is the most abundant NO_x species in the untreated diesel emission, is first oxidized catalytically to NO_2 on the transition metal sites (e.g., Pt or Rh supported by high surface area γ-Al_2O_3 support material) and then stored by the BaO sites as nitrates during the lean cycle. Subsequently, these trapped nitrate species are reduced on the transition metal sites during the rich cycle regenerating the fresh BaO sites for the next catalytic cycle.

There exist only a few surface science studies investigating the fundamental aspects of the NSR catalysts.[8] Design and characterization of model catalyst systems that mimic the critical aspects of a working NSR catalyst is crucial for a molecular level understanding of these interesting catalytic systems which promise a potential industrial alternative to the conventional selective catalytic reduction (SCR) technology.[5] Therefore, in previous reports, our research group investigated the structure[9] and the chemical reactivity of θ-Al_2O_3/NiAl(100) ultrathin films toward H_2O,[9] NO_2,[10] and $NO_2 + H_2O$[11] in the absence of a Ba-containing active component. In this two part series, we focus on the synthesis and characterization of a Ba-containing model NSR catalyst by employing various surface analysis probes. In the first part of this series,[12] we studied Ba deposition on the oxygen-terminated θ-Al_2O_3/NiAl(100) substrate[13−17] under anaerobic conditions. In the second part of the series (i.e., current text), we investigate the oxidation of the deposited Ba species by O_2(g) on the θ-Al_2O_3/NiAl(100) substrate in order to synthesize a model catalyst in the form of BaO/θ-Al_2O_3/NiAl(100), which mimics the active storage component of a realistic NSR catalyst.

2. Experimental Section

The experimental setup and the data acquisition procedures that are employed in the current work are discussed in detail in the first part of this series.[12] Briefly, experiments were performed in an UHV surface analysis chamber ($P_{base} = 2 \times 10^{-10}$ Torr) equipped with facilities for XPS (PHI-dual anode X-ray source, Omicron EA-125 multichannel electrostatic hemispherical electron energy analyzer), AES (PHI-single pass cylindrical mirror analyzer), a quadruple mass spectrometer (QMS, UTI) for TPD, and a rear-view low energy electron diffraction (LEED) setup (Princeton Research Instruments). A custom-made Ba evaporation source, containing an exothermic Ba ring getter material (SAES Getters Inc.) was utilized in the deposition experiments.

3. Results and Discussion

3.1. Ba Deposition and Oxidation Procedures. O_2(g)-assisted Ba oxidation on the θ-Al_2O_3/NiAl(100) substrate is performed using two different preparation methods. In preparation method A, the Ba deposition and subsequent oxidation were carried out in a stepwise fashion. First, a controlled dose of Ba metal was evaporated onto the θ-Al_2O_3/NiAl(100) surface in UHV at 300 K, and then O_2(g) ($P_{O2} = 5 \times 10^{-7}$ Torr) was introduced into the chamber at 300 K. Next, the sample temperature was quickly increased to 800 K in the presence of O_2(g) and the sample was annealed at 800 K for 15 min. After annealing, the sample was cooled to 300 K, O_2(g) was pumped out and XPS data were acquired. These dosing and annealing sequences were repeated for each Ba deposition step in method

* Corresponding author. E-mail: janos.szanyi@pnl.gov

10.1021/jp060669d CCC: $33.50
Published on Web 08/08/2006

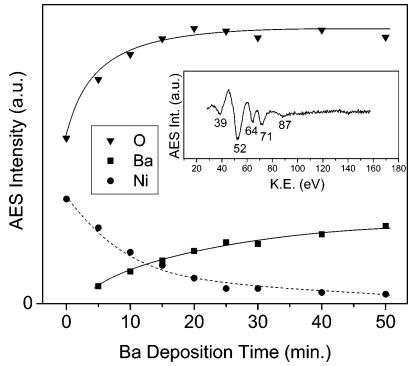

Figure 1. Absolute O_{KLL} (509 eV), Ba_{MNN} (598 eV), and Ni_{LMM} (848 eV) AES intensities for Ba deposition (300 K)/O_2(g) assisted oxidation (800 K) steps on θ-Al_2O_3/NiAl(100) (see text for details). Inset presents the low K.E. region of the AES data obtained after the last deposition/oxidation step (i.e., corresponding to a total Ba deposition time of 50 min).

A (total number of deposition/oxidation steps = 8, total time of Ba deposition = 50 min, 1 ML < θ_{Ba}^{total} < 2 ML). In preparation method B, Ba (θ_{Ba} < 2 ML) was deposited onto the θ-Al_2O_3/NiAl(100) surface in a single deposition step at 300 K in UHV. Next, various doses of O_2(g) were introduced into chamber at 300 K and XPS measurements were performed after each given O_2(g) exposure until the surface was saturated with oxygen. Then, the oxygen-saturated surface was annealed at different temperatures (300 K < T < 1260 K, for 15 min at each temperature) in a step-by-step fashion in UHV and evolution of various surface species were monitored via XPS.

3.2. Ba Deposition at 300 K in UHV and Subsequent Annealing in O_2(g) at 800 K. Figure 1 presents absolute AES intensities of O_{KLL} (509 eV), Ba_{MNN} (598 eV), and Ni_{LMM} (848 eV) features as a function of Ba deposition time in preparation method A. It is apparent from Figure 1 that the O_{KLL} AES signal increases until the fifth deposition/oxidation step and stays almost constant after a total Ba deposition time of 20 min. Although Ba_{MNN} signal increases in a monotonic fashion with increasing Ba deposition time, the increase in the Ba_{MNN} signal intensity occurs with a decreasing rate, leading to a nonlinear (convex-shaped) time dependence without an obvious break point. An inverse behavior to this is observed for the Ni_{LMM} signal in which a monotonic decrease in the AES intensity results in a nonlinear (concave-shaped) time-dependence. The results of Figure 1 indicate that Ba deposition/oxidation via method A does not lead to a layer-by-layer growth. In contrast, the lack of a linear time dependence and an obvious break point in the Ba_{MNN} AES signal suggest formation of 2D islands at low Ba loadings and 3D clusters at higher Ba loadings. It should be noted that the growth behavior suggested by Figure 1 is significantly different from the layer-by-layer growth mode observed for room-temperature Ba deposition on θ-Al_2O_3/NiAl(100) in the absence of O_2(g).[12] Apparently, annealing the deposited Ba layer in O_2 environment at 800 K, as described in section 3.1, leads to highly mobile oxidized Ba clusters which sinter to form 3D structures. Thus, these results indicate that the morphology of the deposited Ba species on the θ-Al_2O_3/NiAl(100) substrate can be controlled by varying the surface temperature and the contents of the gas-phase environment during the oxidation process. The inset of Figure 1 provides additional support for these arguments. The AES data presented in the inset is obtained after the last deposition step of preparation method A (i.e., total Ba deposition time = 50 min). Based on the detailed discussion given in the first part of this series,[12] 52, 64, 71, and 87 eV features in the AES data are

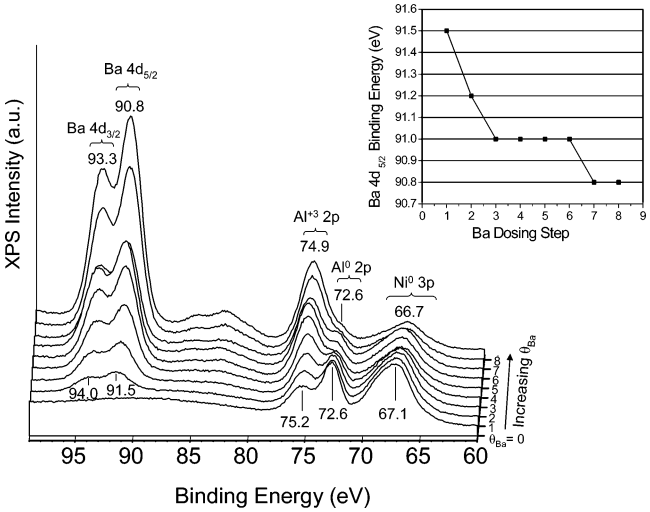

Figure 2. 100−60 eV region of the XPS data for the Ba deposition (300 K)/O_2(g) assisted oxidation (800 K) steps on θ-Al_2O_3/NiAl(100) (see text for details). Inset shows the BE values of the Ba $4d_{5/2}$ feature for each deposition/oxidation step.

predominantly originating from the Ba surface component, although a less significant contribution from the θ-Al_2O_3/NiAl(100) substrate to the 52 and 64 eV features cannot be excluded. Due to the strongly oxidizing conditions that are used in preparation method A, deposited Ba layers are expected to be fully oxidized. It should also be noted that the AES data presented in the inset strongly resemble that of the AES data given in spectrum (v) of Figure 1 in ref 12, where the latter corresponds to Ba layers deposited on the oxygen-terminated θ-Al_2O_3/NiAl(100) surface at 300 K in the absence of O_2(g) and further annealed at 800 K in UHV. Therefore, the similarity between these two cases supports the previous interpretation given in ref 12 that, in the absence of O_2(g), Ba oxidation by alumina substrate continues within 300−800 K where a fully oxidized BaO surface layer is constructed at c.a. 800 K. The feature located at 39 eV in the inset of Figure 1 can be assigned to the Al^{3+} species of the alumina film,[12−13] whereas the minor feature appearing at 87 eVcan be associated with an interdiffusion of Ba−surface component and the underlying alumina substrate.[12]

The 100−60 eV region of the XPS data for preparation method A is presented in Figure 2. The foremost spectrum in Figure 2 corresponds to a clean θ-Al_2O_3/NiAl(100) substrate where Al^{3+} 2p, Al^0 2p, and Ni^0 3p features are visible at 75.2, 72.6, and 67.1 eV, respectively. After the first deposition/oxidation step (total Ba deposition time = 5 min), Ba $4d_{3/2}$ and Ba $4d_{5/2}$ features appear at 94.0 and 91.5 eV, respectively. As the Ba loading is increased, Ba 4d binding energy (BE) values reveal a decreasing trend, with the Ba $4d_{3/2}$ and Ba $4d_{5/2}$ features located at 93.3 and 90.8 eV after the last Ba deposition step (total Ba deposition time = 50 min), respectively. In other words, the BE difference for the Ba 4d levels between the first and the last deposition steps is −0.7 eV. Based on previous theoretical and experimental studies on the BE shifts of Ba in its metallic and oxidized forms,[12,18−25] we attribute this monotonic decrease in BE observed during the Ba deposition on the θ-Al_2O_3/NiAl(100) substrate using preparation method A to the complete oxidation of the Ba layer and the formation of BaO. The Al 2p levels of the θ-Al_2O_3/NiAl(100) substrate also reveal significant changes during the Ba deposition/oxidation in preparation method A. It is clearly seen in Figure 2 that the increasing Ba loading and subsequent oxidation with O_2(g) cause a continuous attenuation of the Al^0 2p feature of the underlying

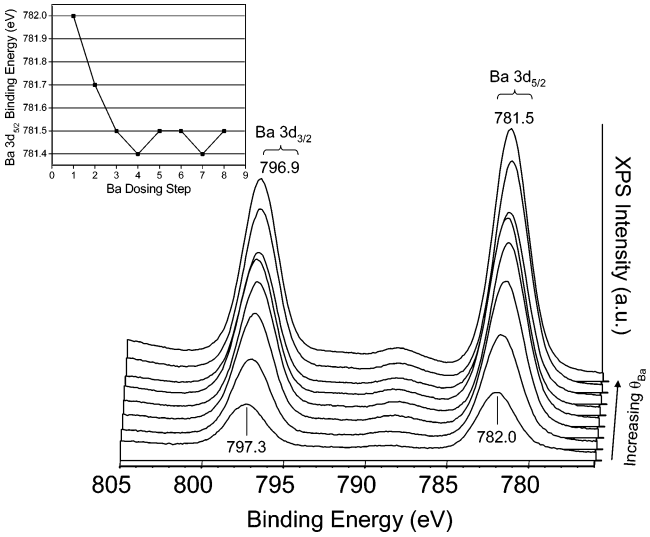

Figure 3. Ba 3d region of the XPS data for the Ba deposition (300 K)/O_2(g) assisted oxidation (800 K) steps on θ-Al_2O_3/NiAl(100) (see text for details). Inset shows the BE values of the Ba $3d_{5/2}$ feature for each deposition/oxidation step.

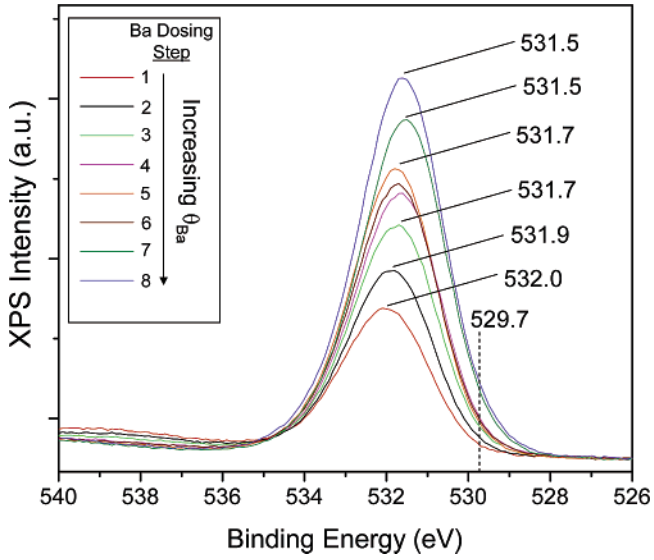

Figure 4. Evolution of the O 1s signal in XPS during the Ba deposition (300 K)/O_2(g) assisted oxidation (800 K) steps on θ-Al_2O_3/NiAl(100) (see text for details).

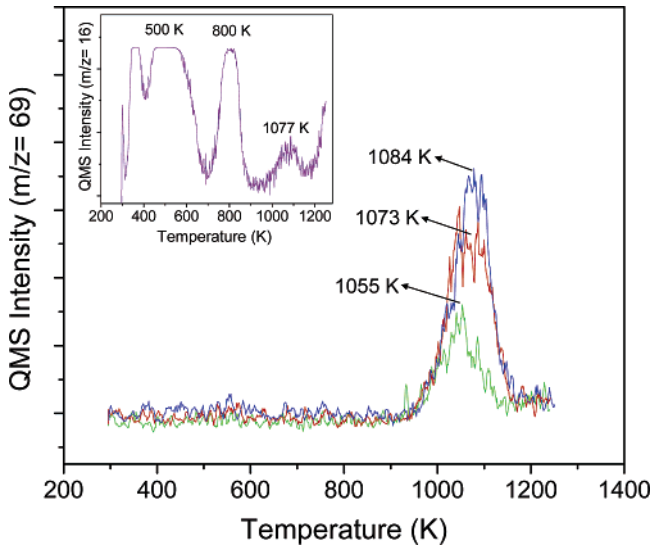

Figure 5. Ba desorption signal in TPD for various coverages of Ba (θ_{Ba} < 5 ML) deposited on the θ-Al_2O_3/NiAl(100) substrate and saturated with O_2(g) at 300 K. Inset shows a representative 16 amu signal originating from O_2 desorption that is simultaneously monitored together with the Ba signal.

NiAl(100) bimetallic substrate. This is an expected result, as the increasing thickness of the BaO/θ-Al_2O_3 overlayer should decrease the number of Al^0 2p photoelectrons that can penetrate the BaO/θ-Al_2O_3 overlayer and leave the sample surface. For a constant θ-Al_2O_3 ultrathin film thickness, a similar phenomenon should also be observed for the Al^{3+} 2p levels (see for example, Figure 4 in ref 12). However, the observed continual increase in the intensity of the Al^{3+} 2p feature in Figure 2 of the current text suggests that the structure of the θ-Al_2O_3/NiAl(100) surface is also changed with increasing number of deposition/oxidation steps. It is well known in the literature that Ba has a promotional effect on the oxidation of semiconductor surfaces, and it has been reported that Ba addition improves the low-temperature O_2(g) assisted Si oxidation rate up to a factor of 5.[26] Based on this information, the increase in the Al^{3+} 2p levels of the alumina film is associated with the thickening (and probably reconstruction/disordering) of the θ-Al_2O_3/NiAl(100) ultrathin film. It should also be mentioned that after the last deposition step, a lack of long-range order of the surface was observed by LEED.

Qualitatively, a similar BE trend is visible for the Ba 3d core levels during the Ba deposition/oxidation via preparation method A, as illustrated in Figure 3. After the first step, Ba $3d_{3/2}$ and Ba $3d_{5/2}$ levels appear at 797.3 and 782.0 eV, respectively, and they shift by approximately −0.6 eV at the end of the last Ba deposition/oxidation step. This behavior is also in agreement with the growth of an oxidized Ba layer in the form of BaO.

The O 1s region of the XPS data obtained during the Ba deposition/oxidation steps of preparation method A is given in Figure 4. The most striking aspect of Figure 4 is the constant increase in the O 1s signal with a relatively symmetric line shape. It was shown in the first part of this series[12] that partially oxidized and disordered Ba layers results in a well-resolved O 1s feature at 529.7 eV. The lack of such a well-resolved feature in Figure 4 implies that the increasing O 1s signal should be due to a combination of the thickening of the alumina film and the growth of a different O-containing phase. Based on the XPS data given above, we assign this O-containing phase to fully oxidized BaO layer. As the maxima of the convoluted O 1s signal shifts to lower BE values with increasing Ba loading, the BaO phase should have a BE value within 532.0 and 530.0 eV. This BE interval assigned for a completely oxidized BaO layer is also consistent with the O 1s shifts given in Figure 11 of ref 12 where deposited Ba metal is oxidized by the alumina substrate at 800 K.

3.3. Decomposition and Desorption of the Oxidized Ba Layer via TPD. Figure 5 illustrates the results of the TPD experiments where the model catalyst surfaces were prepared as follows. Various coverages of Ba metal ($\theta_{Ba} \leq 5$ ML) were deposited on the θ-Al_2O_3/NiAl(100) substrate at 300 K in UHV. Subsequently, the surface was exposed to 9000 L (1 L = 1×10^{-6} Torr sec^{-1}) O_2 (g) at 300 K in order to saturate the surface with oxygen. TPD experiments were performed after having saturated the surface with oxygen. The Ba desorption signal (69 amu signal originating from doubly ionized Ba^{2+} ions in the QMS) is given in Figure 5. Within the thermal window of the TPD experiments (i.e. 300 K− 1250 K), only a single Ba desorption feature is apparent which reveals a zero order desorption kinetics with overlapping leading edges. The desorption maxima for this feature increase with increasing Ba loading and are located within 1055−1084 K for the Ba

coverages studied here. The most important aspect of the TPD data shown in Figure 5 is the lack of any additional Ba desorption signal at $T < 900$ K. This observation suggests that Ba deposits treated with O_2(g) show a significantly different behavior with respect to Ba deposits that are not exposed to O_2(g) (see Figure 7 of ref 12). It should be noted that the incomplete oxidation of thick Ba layers ($\theta_{Ba} < 10$ ML) on the θ-Al_2O_3/NiAl(100) surface in the absence of gas-phase O_2 leads to an intense Ba desorption feature at c.a. 700 K in TPD, which was attributed to the desorption of metallic Ba surface species.[12] In these TPD experiments,[12] additional and less intense desorption features were also observed at $T > 900$ K and were attributed to desorption/decomposition of fully oxidized (BaO) species that are formed at higher temperatures during the TPD experiment. Therefore, the TPD results presented in the current work provide additional support for the previous observations given in the first part of this series,[12] suggesting that saturating the Ba deposits ($\theta_{Ba} \leq 5$ ML) on the θ-Al_2O_3/NiAl(100) substrate with O_2(g) and annealing at higher temperatures ($T \geq 800$ K) results in a more stable, oxidized Ba species that shows significantly different chemical and structural properties with respect to that obtained by Ba deposition ($\theta_{Ba} < 10$ ML) at 300 K in UHV in the absence of O_2(g). For the latter case, due to the lack of a sufficient amount of oxygen, the majority of Ba on θ-Al_2O_3/NiAl(100) desorbs before it is completely oxidized to form stable BaO species. However, even in the absence of gas-phase O_2, the alumina substrate is capable of inducing the formation of BaO species that desorb at $T > 900$ K. As will be shown below, even after annealing at 1260 K, desorption of the Ba species is not completed and a small amount of Ba still exists on/in the substrate surface.

The inset of Figure 5 illustrates a representative O_2 desorption signal that is simultaneously obtained with the Ba desorption signal, implying structural changes in the oxygen saturated Ba layer during the temperature ramp. Although no Ba desorption signal is visible at $T < 950$ K in Figure 5, oxygen desorption features appear, suggesting that the oxygen-saturated Ba layer undergoes structural transformations before its desorption. A more detailed discussion of the relevance of these oxygen desorption features will be presented in section 3.4 in conjunction with complimentary XPS results. Briefly, a broad and intense oxygen desorption feature is visible within 400−700 K, followed by a less intense but sharper feature at 800 K. In addition to these features, a relatively smaller oxygen desorption is also apparent in the inset of Figure 5 which is centered at 1077 K.

3.4. Ba Deposition and O_2 Exposure at 300 K and Subsequent Annealing within 300−1260 K. Figure 6 shows the O 1s region of the XPS data obtained for exposing controlled doses of O_2(g) at 300 K onto a Ba($\theta_{Ba} < 2$ ML)/θ-Al_2O_3/NiAl(100) surface obtained by room-temperature evaporation of Ba as described in section 3.1. The XPS spectrum corresponding to the surface prior to the O_2(g) exposure reveals two major features at 532.5 and 529.7 eV. As described in the first part of this series,[12] the former feature is predominantly due to the O 1s signal of the alumina substrate with some contribution from additional O 1s states that are not in direct interaction with the deposited Ba species, whereas the latter feature is assigned to O 1s species that are associated with a disordered network of partially oxidized Ba phase on the alumina film. With increasing O_2 exposure, an interesting behavior is observed in the O 1s XPS signal. Increasing O_2 exposure results in an obvious intensity transfer from the 529.7 eV feature to the 532.5 eV feature with a concomitant positive BE shift of the latter feature

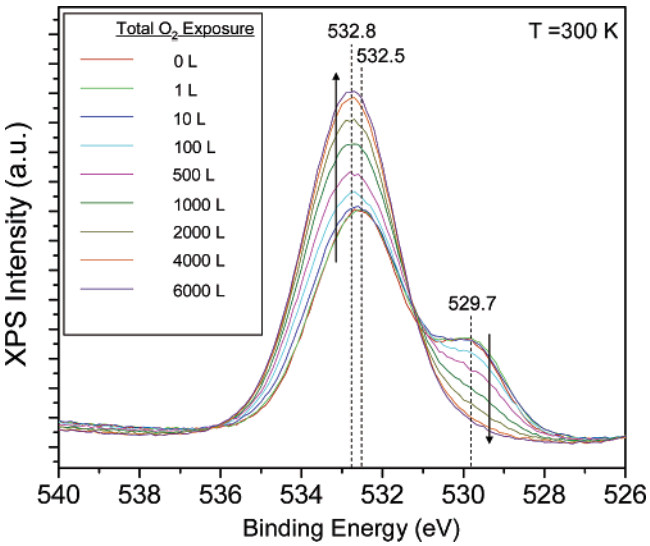

Figure 6. O 1s signal in XPS for a Ba layer ($\theta_{Ba} < 2$ ML) deposited on θ-Al_2O_3/NiAl(100) at 300 K in UHV and exposed to the given O_2 exposures at 300 K.

to 532.8 eV. This intensity transfer, which reflects itself with the presence of an apparent isosbestic point located at 531.2 eV, signifies the transformation of the O 1s state at 529.7 to a new chemical state at 532.8 eV. It is worth mentioning that the Al^{3+} 2p signal (not shown), which is simultaneously monitored for each of the spectra given in Figure 6, shows a monotonic attenuation of the Al^{3+} 2p intensity with increasing O_2 exposure. This observation rules out the possibility of the room-temperature oxidation of the Al^0 sites of the NiAl(100) bimetallic substrate and a subsequent increase in the alumina film thickness. In a number of previous studies, where the interaction of O_2(g) with BaO surfaces was studied via in-situ Raman spectroscopy,[28−29] X-ray diffraction (XRD),[28−29] XPS,[30] and scanning tunneling microscopy (STM),[8] formation of a BaO_2 (barium peroxide) phase was reported. Formation of peroxides (O_2^{2-}) and even superoxides (O_2^-) are also commonly observed for alkali group metals such as Cs.[31] In XPS, peroxide (O_2^{2-}) species typically appear at higher BE values than that of the oxide (O^{2-}) states.[30] Therefore, we assign the intensity transfer from the 529.7 eV feature to the 532.8 eV feature as arising from the conversion of the oxide O 1s states in the disordered network of oxidized Ba to peroxide-like states upon saturation of the surface with O_2(g) at 300 K. It can be seen in Figure 6 that the surface is essentially completely saturated after an O_2 exposure of 6000 L.

Ba 3d levels of the surface Ba component also undergo significant changes during the transformation from the oxide to peroxide states. Figure 7 indicates that the saturation of the surface with O_2(g) at 300 K in preparation method B brings about a positive ΔBE of 0.7 eV with respect to that of the surface prior to O_2 exposure.

In preparation method B, after the saturation of the Ba deposit with O_2 at room temperature, annealing experiments were performed, and structural transformations of the surface were monitored using XPS. Figure 8 presents the O 1s region of the XPS data from these experiments. At 300 K, as described above, the O_2 saturated surface shows a relatively symmetric but a convoluted line shape as a result of the presence of peroxide-like O 1s states as well as the oxide states of the alumina substrate (532.8 eV). Within 300−600 K, annealing leads to broadening of the 532.8 eV feature and reappearance of the 529.7 eV shoulder. This is not surprising as the O_2 desorption

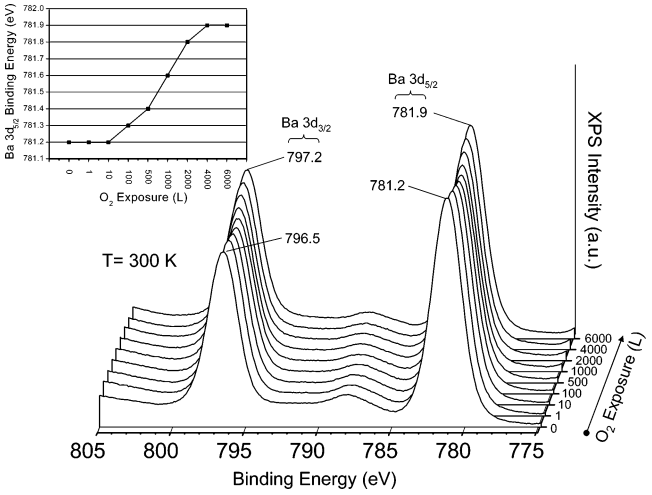

Figure 7. Ba 3d signal in XPS for a Ba layer (θ_{Ba} < 2 ML) deposited on θ-Al_2O_3/NiAl(100) at 300 K in UHV and exposed to the given O_2 exposures at 300 K.

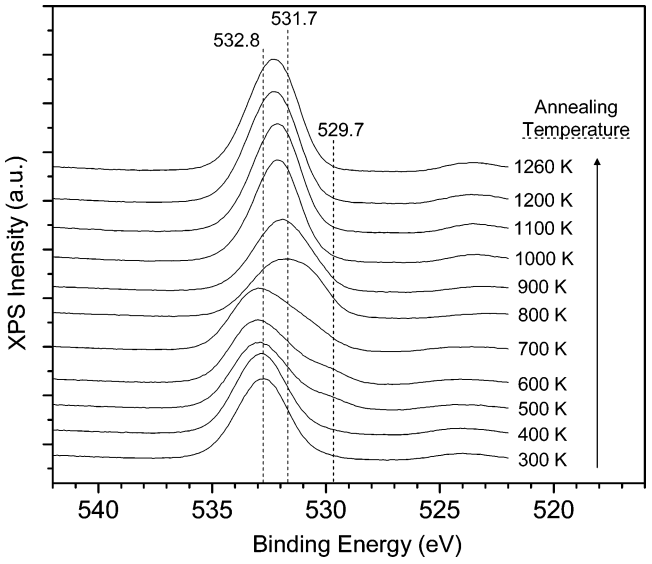

Figure 8. O 1s signal in XPS during the annealing of a Ba layer (θ_{Ba} < 2 ML) deposited on θ-Al_2O_3/NiAl(100) at 300 K in UHV and saturated with O_2 at 300 K.

signal that is monitored during the TPD experiments of Figure 5 reveals a broad desorption feature within 300−600 K, suggesting a loss of oxygen from the surface to vacuum via desorption. This observation is consistent with the transformation of the peroxide states to oxide states due to O_2 desorption. Within 700−800 K, a very significant attenuation of the high BE feature and a considerable broadening of the overall O 1s signal is visible in Figure 8. It should be emphasized that Ba desorption from the surface does not occur within this thermal window (Figure 5); thus, the changes that are observed in Figure 8 at 700−800 K should be associated with structural changes rather than coverage-dependent changes due to Ba desorption. We attribute these changes to the formation of a completely oxidized BaO layer. At T > 900 K, indications of Ba desorption from the surface start to appear (see also Figure 9), as a result of the decomposition of the BaO layer. As the surface Ba coverage decreases, the O 1s states originating from the alumina substrate start to dominate. The observation of an oxygen desorption signal at 1077 K in Figure 5 is also in line with the BaO decomposition. Finally at 1260 K, the O 1s signal assumes

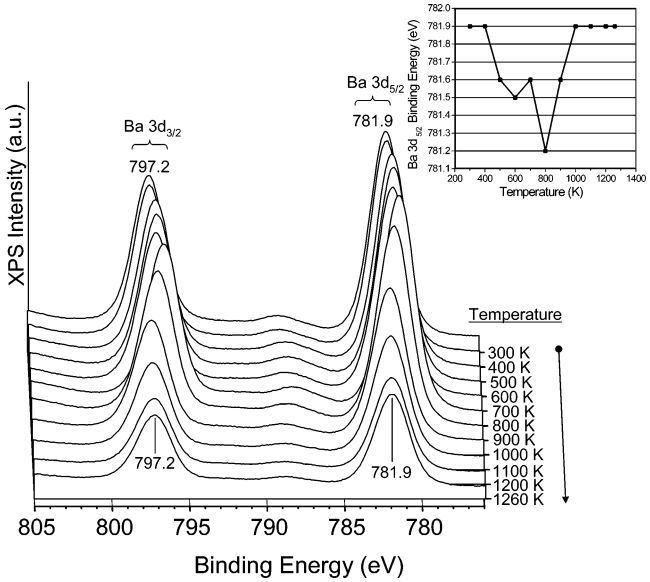

Figure 9. Ba 3d signal in XPS during the annealing of a Ba layer (θ_{Ba} < 2 ML) deposited on θ-Al_2O_3/NiAl(100) at 300 K in UHV and saturated with O_2 at 300 K. Inset shows the changes in the BE values of the Ba $3d_{5/2}$ feature at each annealing temperature.

a more symmetrical line shape and is centered at 532.2 eV, similar to that of the Ba-free alumina substrate.

The Ba 3d region of the XPS data (Figure 9) provides additional insights into the structural transformations presented in Figure 8. The oxygen saturated surface is given at 300 K in the topmost spectrum with a Ba $3d_{5/2}$ feature located at 781.9 eV. The inset of Figure 9 enables a detailed analysis of the BE changes of the Ba $3d_{5/2}$ feature during the annealing steps. It is apparent from the inset that the annealing steps within 400−800 K result in a decreasing trend in the BE values of the Ba $3d_{5/2}$ feature, which can be explained by the destruction of the peroxide states and the formation of a relatively ordered BaO network on the substrate surface. On the other hand, annealing steps at T > 800 K leads to loss of both Ba (Figure 9) and O (Figures 5 and 8) from the surface and results in an increase in the BE of the Ba $3d_{5/2}$ feature that is consistent with a decrease in Ba surface coverage (see Figure 3 above and also Figure 5 of ref 12).

4. Summary and Conclusions

In this work we investigated Ba deposition on a θ-Al_2O_3/NiAl(100) substrate and its oxidation with gas-phase O_2 at various surface temperatures using different surface analysis probes. Our results can be summarized as follows.

(a) Preparation of an oxidized Ba deposit by oxidation in O_2 at 800 K results in the growth of 2D and 3D Ba-containing surface domains, rather than a layer-by-layer growth mode. Combined with the previous results discussed in the first part of this series,[12] where a layer-by-layer growth of partially oxidized Ba layers was obtained using a different preparation protocol, it is apparent that the growth morphology and the oxidation state of the Ba species on the θ-Al_2O_3/NiAl(100) substrate can be fine-tuned by controlling preparation conditions such as surface temperature and gas-phase composition.

(b) Ba deposits prepared by oxidation with O_2(g) at 800 K lead to the formation of a fully oxidized BaO surface network.

(c) Saturation of a Ba deposit with O_2(g) at room temperature reveals the formation of BaO_2-like surface states. These metastable peroxide (O_2^{2-}) states are converted to regular oxide (O^{2-}) states of BaO at higher temperatures (800 K).

(d) In terms of thermal stability, BaO surface layers that are formed by O_2(g) assisted oxidation on the θ-Al_2O_3/NiAl(100) substrate are significantly more stable (with a desorption/decomposition temperature of c.a. 1050 K) compared to the thick Ba layers ($2 < \theta_{Ba} < 10$ ML) deposited under anaerobic conditions described in the first part of this series, whose multilayer desorption features appear as low as 700 K.

Acknowledgment. We gratefully acknowledge the U.S. Department of Energy (DOE), Office of Basic Energy Sciences, Division of Chemical Sciences for the support of this work. The research described in this paper was performed at the Environmental Molecular Sciences Laboratory (EMSL), a national scientific user facility sponsored by the DOE Office of Biological and Environmental Research and located at Pacific Northwest National Laboratory (PNNL). PNNL is operated for the U.S. DOE by Battelle Memorial Institute under contract number DE-AC05-76RL01830. The authors acknowledge with pleasure Drs. Zdenek Dohnálek and Mark Engelhard for helpful discussions.

References and Notes

(1) Newmann, N.; Lyons, W. G. *J. Supercond.* **1993**, *6*, 119.
(2) Radousky, H. B. *J. Mater. Res.* **1992**, *7*, 1917.
(3) Weitering, H. H. *Surf. Sci.* **1996**, *355*, L271.
(4) Cho, W. S.; Kim, J. Y.; Kim, S. S.; Choi, D. S.; Jeong, K.; Lyo, I. W.; Whang, C. N.; Chae, K. H. *Surf. Sci.* **2001**, *476*, L259.
(5) Heck, R. M.; Farrauto, R. J. *Catalytic Air Pollution Control: Commercial Technology;* International Thomson Publishing: New York, 1995.
(6) Matsumoto, S. *Cattech.* **2000**, *4*, 102.
(7) Epling, W. S.; Campbell, L. E.; Yezerets, A.; Currier, N. W.; Parks, J. E., II *Catal. Rev.* **2004**, *46*, 2, 163 and references therein.
(8) Stone, P.; Ishii, M.; Bowker, M. *Surf. Sci.* **2003**, *537*, 179.
(9) Ozensoy, E.; Szanyi, J.; Peden, C. H. F. *J. Phys. Chem. B* **2005**, *109*, 3431.
(10) Ozensoy, E.; Peden, C. H. F.; Szanyi, J.; *J. Phys. Chem. B* **2005**, *109*, 15977.
(11) Ozensoy, E.; Peden, C. H. F.; Szanyi, J.; *J. Phys. Chem. B* **2006,** *110*, 8025.
(12) Ozensoy, E.; Peden, C. H. F.; Szanyi, J. *J. Phys. Chem. B* **2006**, *110*, 17001.
(13) Gassmann, P.; Franchy, R.; Ibach, H. *Surf. Sci.* **1994**, *319*, 95.
(14) Gassmann, P.; Franchy, R.; Ibach, H. *J. Electron Spectrosc. Relat. Phenom.* **1993**, *64/65*, 315.
(15) Fremy, N.; Maurice, V.; Marcus, P. *J. Am. Ceram. Soc.* **2003**, *86*, 669.
(16) Fremy, N.; Maurice, V.; Marcus, P. *Surf. Interface Anal.* **2002**, *34*, 519.
(17) Maurice, V.; Fremy, N.; Marcus. P. *Surf. Sci.* **2005**, *581*, 88.
(18) Lampert, W. V.; Rachocki, K. D.; Lamartine, B. C.; Haas, T. W. *J. Electron Spectrosc. Relat. Phenom.* **1982**, *26*, 133.
(19) Van Doveren, H.; Verhoeven, J. A. Th. *J. Electron Spectrosc. Relat. Phenom.* **1980**, *21*, 265.
(20) Wertheim, G. K. *J. Electron Spectrosc. Relat. Phenom.* **1980**, *34*, 309.
(21) Jacobi, K.; Astaldi, C.; Frick, B.; Geng, P. *Phys. Rev. B* **1987**, *36*, 3079.
(22) Barr, T. L. *J. Vac. Sci. Technol. A* **1991**, *9*, 1793.
(23) Hill, D. M.; Meyer, H. M., III; Weaver, J. H. *Surf. Sci.* **1990**, *225*, 63.
(24) Vasquez, R. P. *J. Electron Spectrosc. Relat. Phenom.* **1991**, *56*, 217.
(25) Pacchioni, G.; Sousa, C.; Illas, F.; Parmigiani, F.; Bagus, P. S. *Phys. Rev. B* **1993**, *48*, 11573.
(26) Mesarwi, A.; Ignatiev, A. *J. Vac. Sci. Technol. A* **1991**, *9*, 2264.
(27) Wu, Y.; Garfunkel, E.; Madey, T. E. *Surf. Sci.* **1996**, *365*, 337.
(28) Hess, C.; Lunsford J. H. *J. Phys. Chem. B* **2002**, *106*, 6358.
(29) Hess, C.; Lunsford J. H. *J. Phys. Chem. B* **2003**, *107*, 1982.
(30) Dissanayake, D.; Lunsford J. H.; Rosynek, M. P. *J. Catal.* **1993**, *143*, 286.
(31) Hrbek, J.; Yang, Y. W.; Rodriguez, J. A. *Surf. Sci.* **1993**, *296*, 164.